Oxygen vibrations and acoustic surface plasmon on Be(0001)

M. Jahn,[*] M. Müller, M. Endlich, N. Néel, and J. Kröger[†]

Institut für Physik, Technische Universität Ilmenau, D-98693 Ilmenau, Germany

V. Chis

Donostia International Physics Center (DIPC), Donostia-San Sebastián ES-20018, Basque Country, Spain

B. Hellsing

Department of Physics, Göteborg University, S-41296 Göteborg, Sweden

(Received 2 June 2012; published 28 August 2012)

Spectroscopic signatures of vibrational excitations on initially oxidized Be(0001) are identified by a combination of electron energy loss spectroscopy and density functional calculations. Prominent spectral features are due to vibrations in a Be-O mixing layer. Scanning tunneling microscopy indicates that initial oxidation occurs locally in the form of islands. The acoustic surface plasmon persists on the oxygen-covered surface. Its dispersion has been determined along the $\bar{\Gamma}\bar{K}$ direction and is virtually identical to the dispersion of the acoustic surface plasmon of the clean surface.

I. INTRODUCTION

The interaction of oxygen with metal surfaces is a topic of scientific and technological interest.[1,2] Indeed, the oxidation of metals is a universal reaction since the oxide of most metals is more stable than the metal itself.[3] The case of beryllium is particularly interesting since its surface can be easily oxidized even at low temperatures and in ultrahigh vacuum.[4–8] Among many other technologically relevant properties, e.g., high melting point and low weight,[9] its easy oxidation has made beryllium a preferred getter material for oxygen and water in nuclear fusion reactors.[6,10] Owing to the general interest in fundamental processes occurring during metal oxidation and to the specific properties of beryllium it is not surprising that O_2 adsorption to Be surfaces has been investigated to some extent. A few experimental studies based on photoelectron and Auger electron spectroscopy reveal that surface oxidation begins at oxidation nucleation centers with subsequent lateral growth.[4–8] Oxidation of Be can likewise occur via the dissociative adsorption of H_2O in a wide temperature range.[6,11,12] In particular, at room temperature the H_2O molecules dissociate completely and oxidize the surface by oxide island nucleation and growth.[6] Less theoretical work on Be oxidation is available.[13,14] These studies[13,14] consistently report that oxidation proceeds via the dissociative adsorption of O_2 molecules. Based on adsorption energy calculations a possible incorporation of O atoms into the Be(0001) surface has been suggested.[14]

The (0001) surface of Be has further attracted considerable attention owing to the existence of a two-dimensional plasmon with soundlike dispersion, which is referred to as an acoustic surface plasmon.[15,16] In general, this kind of collective electron excitation exhibits low energies and is thus likely to participate in electron-phonon coupling phenomena such as superconductivity[17,18] and in electron-photon interactions, which are the basis of plasmonics.[19,20] The prerequisite for the occurrence of an acoustic surface plasmon is the coexistence of a partially occupied surface state band and the continuum of bulk electrons.[15,16] Indeed, acoustic surface plasmons have

been predicted for the (111) noble metal surfaces,[21] which host a Shockley surface state, and for Ag thin films.[22] So far, they have been observed experimentally on Au(111) (Ref. 23) and Cu(111).[24] Experimental evidence for surface acoustic plasmons has also been reported for metallic nanoparticles[25] and for epitaxial graphene on Pt(111).[26] Since electronic surface states are significantly affected by even small amounts of adsorbates,[27] a question arises as to the influence of adsorbates on acoustic surface plasmons. However, this question has been scarcely investigated. At present alkali-metal adsorption on Be(0001) has been shown to distort the dispersion due to induced quantum well states.[28–30] It has been demonstrated in Ref. 16 that increasing exposure of Be(0001) to O_2 leads to a shift of the surface plasmon energy and a decrease of its intensity in vibration spectra acquired along the $\bar{\Gamma}\bar{M}$ direction of the surface Brillouin zone.

In this article, vibrational spectroscopy with inelastically scattered electrons is combined with density functional calculations to provide a clear-cut identification of oxygen vibration modes along with a proposed structure of initially oxidized Be(0001). Energy loss features in specular spectra are identified as signatures of vibrational excitations in a Be-O mixing layer. At the initial stage of oxidation the mixing layer occurs as separated Be-O islands as suggested by scanning tunneling microscopy (STM) images recorded at room temperature. In addition, the dispersion of the acoustic surface plasmon has been determined along the $\bar{\Gamma}\bar{K}$ direction of the Be(0001) surface Brillouin zone. Comparison with calculated dispersion data for clean Be(0001) (Ref. 16) reveals that the dispersion is virtually not affected by the initial oxidation.

II. EXPERIMENTAL AND THEORETICAL METHODS

Experiments were performed with an Ibach-type spectrometer[31] in ultrahigh vacuum with a base pressure of 10^{-8} Pa and at room temperature. The incident monochromatic electron beam encloses an angle of $65°$ with the surface normal.

The energy resolution of the spectrometer was set to 3–7 meV depending on the intensity of the vibrational signals. Dispersion data were acquired by angle-resolved measurements with a wave-vector resolution of $0.01\,\text{Å}^{-1}$. To this end the analyzer of the spectrometer was rotated out of the specular scattering direction. After introducing the Be sample into the vacuum recipient a thick oxide film had to be removed by repeated cycles of Ar^+ bombardment and annealing. The progressive reduction of the oxide film thickness was monitored by x-ray photoelectron spectroscopy. Crystalline order was checked by low-energy electron diffraction and cleanliness by specular electron-energy-loss spectra. The crystal was exposed to O_2 and H_2 at room temperature by backfilling the recipient to 10^{-6} Pa (O_2) and 10^{-5} Pa (H_2) of the highly purified (purity 99.995%) gases.

Total energy calculations were performed within the framework of density functional theory (DFT) employing ultrasoft pseudopotentials and the Perdew-Burke-Ernzerhof[32,33] general gradient approximation to the exchange and correlation energy functional. The dynamical properties at the $\bar{\Gamma}$ point were calculated by applying density functional perturbation theory (DFPT) included in the QUANTUM-ESPRESSO[34] package. The electron wave functions were expanded in plane waves with an energy cutoff of 32 Ry (1 Ry = 13.6 eV), while for the effective potential and the charge density an energy cutoff of 288 Ry was used. The integration over the surface Brillouin zone was carried out over a $(8 \times 8 \times 1)$ Monkhorst-Pack division of the **k** points, and a finite temperature smearing of the Marzari-Vanderbilt[35] type set to 0.03 Ry. The atomic arrangement was obtained by minimizing the total energy with respect to the positions of the atoms. The working slab includes 14 $(\sqrt{3} \times \sqrt{3})$-Be(0001) layers (3 Be atoms in each layer) and two oxygen atoms on each side of the slab surface. Each repeated slab was separated by 18 Å of vacuum perpendicular to the surface. The structure was optimized without any constraints on symmetry until the resulting forces acting on individual atoms were less than $25\,\text{meV}\,\text{Å}^{-1}$.

III. RESULTS AND DISCUSSION

A. Oxygen vibrations

Figure 1 shows the time evolution of vibrational spectra acquired from Be(0001) in specular scattering geometry. A sharp feature at 20 meV and rather weak and broad signatures at 42 and 110 meV have been observed 1 h after the last cleaning cycle (bottom line in Fig. 1). Calculations (see below) reveal that peaks at 20 and 42 meV are due to Be vibrations, while spectral weight at 110 meV originates from vibrations in a Be-O mixing layer. While the peaks at 20 and 42 meV become slightly weaker within 60 h the spectra at higher vibration energies exhibit considerable changes. Starting from 10 h in ultrahigh vacuum, spectra from Be(0001) surfaces exhibit a loss peak at 72 meV, which with increasing time exhibits an increasing vibrational energy. After 50 h a further energy increase fell below the detection limit. Similar energy shifts have been reported for dipole-active perpendicular Li vibration modes on various metal surfaces in the low-coverage range.[36–38] This energy increase has been interpreted in terms of dipole-dipole interactions between the
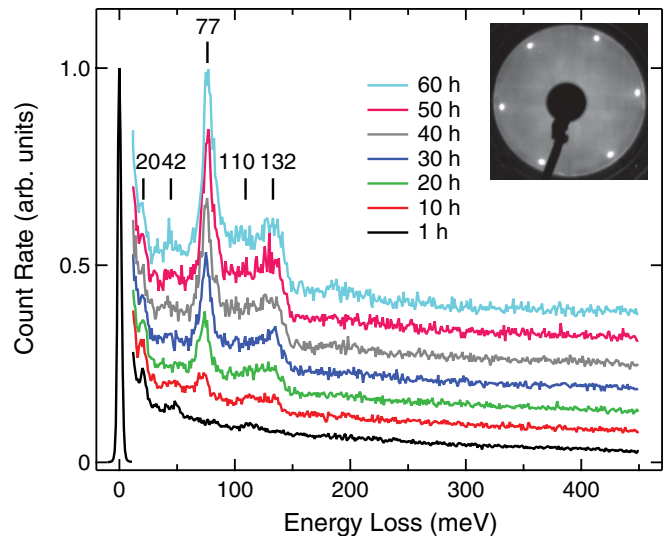
FIG. 1. (Color online) Time evolution of electron-energy-loss spectra acquired from Be(0001) in specular scattering geometry with an electron primary energy of 8 eV. The count rate of the elastic peak is 70×10^3 s^{-1}. Loss spectra have been multiplied by 750 and vertically offset. The full width at half maximum (FWHM) of the elastic peak is 4 meV. Inset: Low-energy electron diffraction pattern of clean Be(0001) acquired with an electron kinetic energy of 112 eV.

adsorbed alkali-metal atoms. A similar scenario may hold here since the vibration mode at 77 meV predominantly exhibits vertical displacement patterns (see below). An additional broad contribution appears at 132 meV starting from 10 h after the last cleaning cycle and likewise increases in intensity. The initially observed spectral feature at 110 meV is hardly discernible since it is flanked by the increasingly strong peak at 77 meV and the rather broad feature at 132 meV. For energies exceeding 150 meV the specular loss spectra remain virtually featureless. A faint feature around 180 meV becomes discernible after 60 h and may be due to the presence of atomic hydrogen.[39] Off-specular loss spectra acquired from Be(0001) that stayed in ultrahigh vacuum for more than 10 h exhibit additional features in an energy range of 150–450 meV. These loss features are most likely the spectroscopic signatures of H and OH vibration modes (see below). As a first result, cleanliness of Be(0001) degrades on a time scale of 10 h.

To identify the origin of the spectroscopic signatures presented in Fig. 1 clean Be(0001) was exposed to O_2. The reason for choosing O_2 is the easy oxidation of Be, which in ultrahigh vacuum occurs via dissociative adsorption of residual H_2O.[40] The top vibrational spectrum presented in Fig. 2 is a specular spectrum acquired from Be(0001) after exposure to 10 L (1 L = 10^{-4} Pa s) O_2, while the bottom spectrum results from a cleaned surface that stayed 60 h in ultrahigh vacuum. Both spectra look similar. Indeed, the most prominent feature in both spectra is a loss peak at 77 meV. Likewise the broad peaks at 110 and 132 meV and the rather sharp decrease of vibrational signal at 150 meV are observed from both spectra. The top spectrum exhibits a slightly higher intensity of the peak at 77 meV which possibly results from a higher oxygen coverage. This interpretation is in line with the higher intensity of the high-energy wing of the peak at 77 meV and that peaks at 20 and 42 meV are hardly
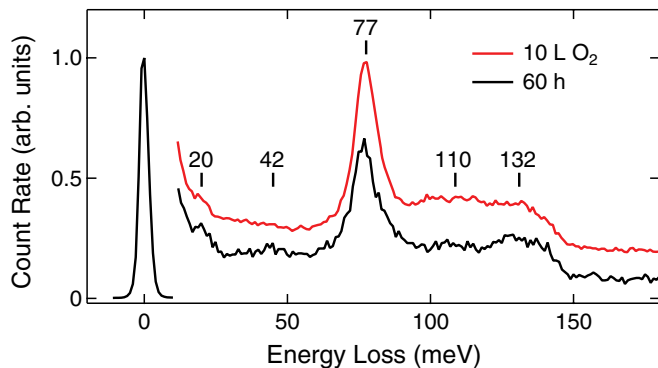
FIG. 2. (Color online) Comparison of specular spectra acquired from clean Be(0001) after exposure to the residual gas of the ultrahigh vacuum for 60 h (bottom) and after exposure to 10 L O_2 (top). The loss spectra were multiplied by 250 and vertically offset. Impact energy: 8 eV (both); count rate of elastic peak: 70×10^3 s^{-1} (bottom) and 120×10^3 s^{-1} (top); FWHM of elastic peak: 4 meV (both).

discernible. The clean sample has likewise been exposed to H_2, which gives the dominant contribution to the mass spectrum of the residual gas in the vacuum recipient. However, even at elevated exposures exceeding 100 L specular vibration spectra are essentially identical with those of the clean surface, i.e., hydrogen in its molecular form does not adsorb on Be(0001) at room temperature. This result is in agreement with earlier findings.[39,41] Exposing clean Be(0001) to atomic hydrogen does lead to adsorption but the resulting vibration spectra of the H-covered surface differ strongly from those of the O_2-exposed sample.[39] Consequently, based on the adsorption experiments contributions to vibration spectra at 77, 110, and 132 meV (Fig. 1) are likely due to oxygen-related vibrations. To unravel the origin of peaks at 20 and 42 meV and to clarify the adsorption structure calculations have been performed.

The proposed structure based on the DFT calculations is illustrated as top [Fig. 3(a)] and side [Fig. 3(b)] views. O and Be atoms appear with red and gray color, respectively. Inequivalent O atoms are denoted O_A and O_B. The dashed line shows the boundaries of the unit cell within the surface plane that has been used in the calculations. The in-plane lattice parameter of this cell is 3.95 Å. The side view [Fig. 3(b)] shows that the topmost Be layer is incorporated in a bilayer of oxygen whose top (bottom) layer is formed by O_A (O_B) atoms. Each oxygen layer (O_A,O_B) exhibits a $(\sqrt{3} \times \sqrt{3}) - R\,30°$ structure, which is referred to the hexagonal structure of the intermediate Be layer. The O_A and O_B lattices are shifted but not rotated with respect to each other (Fig. 3). The separation of O_A and O_B atoms in the surface normal direction (z) is 1.11 Å. The topmost layer (O_A) resides 0.66 Å above the Be layer, while the bottom oxygen layer (O_B) is located 0.45 Å below. In the following, this layer containing Be, O_A, and O_B atoms is referred to as the Be-O mixing layer. The distance between the Be-O mixing layer and the second Be layer is 1.67 Å. Several structures were tested. However, based on (i) the calculated binding energy of the adsorbed oxygen atoms, (ii) the dynamic stability of the structure, and (iii) the fairly good agreement between the calculated and measured phonon spectrum with respect to the energy and relative intensities of four distinct modes to be discussed below, we propose the
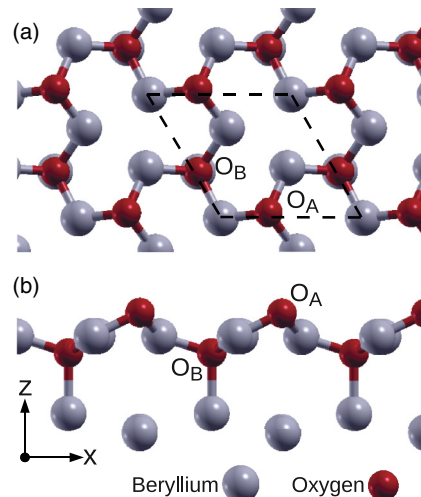
FIG. 3. (Color online) Top (a) and side (b) views of the proposed Be-O mixing layer. The dashed line in (a) indicates the $(\sqrt{3} \times \sqrt{3}) - R\,30°$ unit cell used for the calculations. Inequivalent O atoms are denoted O_A and O_B, which reside atop (O_A) and below (O_B) the topmost Be layer.

atomic structure displayed in Fig. 3. This structure is different from a previously suggested one.[14] Most likely, the $p(3 \times 3)$ O superstructure proposed in Ref. 14 is due to the symmetry of the chosen unit cell in the calculations and may not necessarily be the most stable structure.

The phonon structure is obtained from the DFPT calculations. To ensure the good quality and reliability of the calculations the phonon dispersion relations of clean Be(0001) were calculated. Figure 4 shows a comparison of our calculations with previously reported data.[42] Specifically, the calculated energy of the Rayleigh wave (circles) at the $\bar{M}$ point of the surface Brillouin zone is well reproduced, which is an improvement to a previous report.[42] The dispersion curves reveal that at $\bar{\Gamma}$ a variety of Be modes in an energy range of 6–83 meV are present. Calculated Be vibration modes
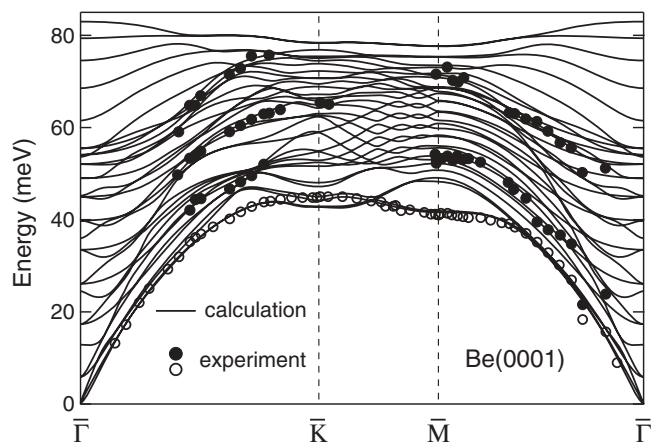
FIG. 4. Calculated phonon dispersion curves of clean Be(0001) along the indicated directions of the surface Brillouin zone. The distance between $\bar{\Gamma}$ and $\bar{M}$ ($\bar{K}$) is 1.59 Å^{-1} (1.84 Å^{-1}). Experimental data appear as circles (Rayleigh wave) and dots and have been adopted from Ref. 42.
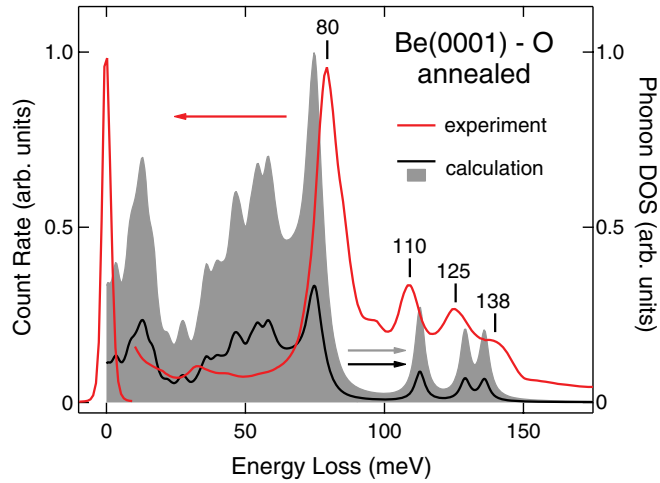
FIG. 5. (Color online) Specular vibration spectrum and calculated phonon DOS of O-covered Be(0001). The spectrum was acquired from a Be(0001) surface after an oxygen exposure of 10 L and subsequent annealing at 600 K for several hours (impact energy: 8 eV; count rate and FWHM of elastic peak: 180×10^3 s^{-1}, 3 meV). The loss spectrum has been multiplied by 50. The shaded area displays the total phonon DOS, while the full line depicts the DOS of phonons with predominant displacements along the surface normal.

FIG. 6. (Color online) Phonon displacement fields within the $(\sqrt{3} \times \sqrt{3}) - $R 30° unit cell for phonon modes at 75 meV (a), 112 meV (b), and 130 meV (c). The relative lengths of the arrows indicate the relative displacements of the atoms.

at 17 and 40 meV may correspond to the experimentally observed loss peaks at 20 and 42 meV in specular spectra (bottom spectrum in Fig. 1). It is tempting to refer the 42 meV peak to the flat Rayleigh mode at $\bar{K}$ of the clean Be(0001) surface Brillouin zone, which due to the oxygen-induced superstructure is backfolded to $\bar{\Gamma}$. However, the structural changes of the beryllium surface layer when oxygen is adsorbed are substantial (Be-O mixing layer, Fig. 3) and most likely wash out the characteristics of the clean Be(0001) surface Rayleigh mode. The absence of the other calculated modes from specular spectra may be due to their weak dynamical dipoles or low excitation cross sections, which vary with the primary energy of impinging electrons.

When atomic oxygen is adsorbed the calculations reveal several vibration modes that are mainly localized in the Be-O mixing layer. The calculated phonon density of states (DOS) at $\bar{\Gamma}$ is plotted along with experimental data acquired in specular scattering geometry from Be(0001) exposed to 10 L of oxygen in Fig. 5. Additionally, the O-covered surface had been annealed at 600 K for several hours prior to data acquisition at room temperature. The annealed surface most likely exhibits a structure that resembles the relaxed structure of the calculations more closely than the surface solely exposed to O$_2$. Together with the total phonon DOS of the Be-O mixing layer (shaded area) contributions from vertical atom displacements are displayed as a full line. The energies of the dominant loss peaks in experimental spectra, i.e., 80, 110, 125, and 138 meV, are closely reproduced by the calculations. The phonon DOS peaks at 75, 112, 130, and 136 meV. The calculated peak at 75 meV exhibits most contributions from shear-vertical displacements, while the three higher energy modes show dominant contributions from displacements in the surface plane. In addition to the accordance between calculated and measured vibration energies the calculated
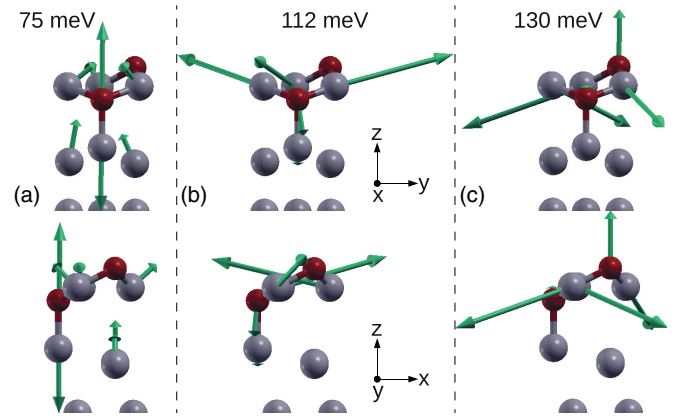
relative intensities of the above-mentioned modes are in qualitative agreement with the experiment.

Figure 6 illustrates the atom displacements, i.e., the predominantly shear-vertical phonon at 75 meV [Fig. 6(a)] and the displacement patterns of vibration modes at 112 [Fig. 6(b)] and 130 meV [Fig. 6(c)], which exhibit strong in-plane contributions. The phonon mode at 75 meV clearly shows large shear-vertical displacements of the O$_B$ atoms together with the Be atom below, while the other atoms have much smaller vertical displacements. The large vertical displacements of the 75 meV mode presumably yield a large dynamical dipole moment perpendicular to the surface plane which then couples strongly to the normal oriented field induced by the dipole-scattered electrons. This may explain the experimentally observed high count rate of this mode in comparison with the high-frequency modes. The smaller vertical atom displacements for the phonon modes at higher energy may be responsible for a smaller dynamic dipole moment, which may explain the experimentally observed low count rate of these modes in specular vibration spectra. The displacement pattern of atoms in the 112-meV mode is very similar to that of the 75-meV mode. However, the in-plane displacements of Be atoms of the topmost layer are much more pronounced than observed from the 75-meV mode. The mode at 130 meV [Fig. 6(c)] likewise gives rise to a spectroscopic signature in vibration spectra. The characteristic of this mode is the O$_A$ atoms having larger vertical displacements than the O$_B$ atoms. Further, the surrounding Be atoms exhibit considerable in-plane motions.

Before discussing the dispersion of the acoustic surface plasmon we comment on two observations. First, the experimentally observed peak at 80 meV (Fig. 5) has slightly shifted from 77 meV measured from samples prior to annealing (Fig. 2). This shift may be caused by structural changes of the oxygen layer induced by annealing. A similar scenario has been proposed for O on Mo(110).[43] Second, low-energy electron diffraction patterns do not show any hint to the $(\sqrt{3} \times \sqrt{3}) - $R 30° superstructure, nor to any other superstructure. Even elevated O$_2$ exposures of 100 L result in diffraction patterns that are virtually identical to the diffraction pattern
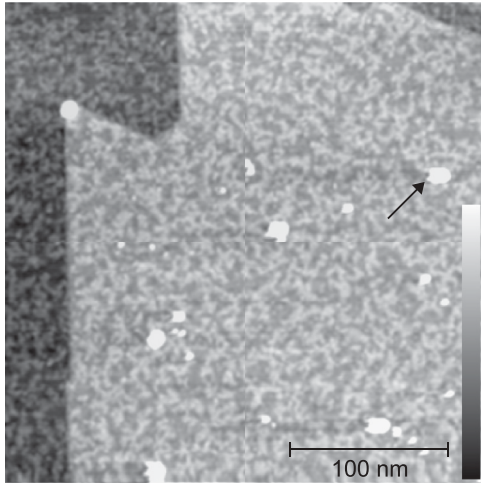
FIG. 7. Constant-current STM image acquired at room temperature from a cleaned Be(0001) surface exposed to 10 L of O_2 (0.5 V, 1 nA). The color scale ranges from apparent heights between 0 and 8.5 Å. Islands with irregular circumference and an average apparent height of 1 Å are assigned to local areas of the Be-O mixing layer. The arrow indicates impurities. Raw data have been smoothed.

of clean Be(0001) (inset of Fig. 1). In particular, no additional diffraction spots appeared, which would be expected for a superstructure with long-range periodicity. This observation is in agreement with an earlier investigation into low-energy electron diffraction patterns of initially oxidized Be(0001).[5] It has been shown in Ref. 5 that room-temperature deposition of oxygen does not lead to additional diffraction patterns up to 120 L. Only annealing samples exposed to $\approx$100 L at $\approx$700 K results in additional diffraction beams. These findings were interpreted in terms of randomly arranged bulklike BeO nuclei at submonolayer oxygen coverages by which initial oxidation of the surface proceeds.

STM images of Be(0001) exposed to small amounts of O_2 do not exhibit structures with long-range order. Figure 7 shows a typical STM image of Be(0001) exposed to 10 L of O_2.[44] Two adjacent substrate terraces are visible, on which irregularly shaped protrusions are distributed. We assign these structures to local areas of oxidized Be(0001) for several reasons. Similar structures were reported from metal surfaces exposed to O_2 at room temperature, i.e., Pt(111),[45] Cr(110),[46] Mg(0001),[47] and Pt(110).[48] Further, increasing the exposure of Be(0001) to O_2 leads to an increased amount of islands that partly coalesce and thus increase the coverage of the observed structures. In addition, the protrusions appear with an average apparent height of 1 Å. The calculated distance between the topmost O and the first Be layer in the Be-O mixing layer (Fig. 3) is 0.66 Å. Comparing apparent heights from STM images with geometric distances is difficult due to the voltage dependence of STM data. However, between 0.4 and 1.6 V the apparent height of the islands did not vary considerably. Extending the voltage range in particular to negative voltages was hampered by unstable imaging conditions. Obviously, the Be-O islands do not form a closed film and no long-range ordered patterns are visible, which is probably the origin of the missing diffraction pattern of the superstructure.

To our knowledge Fig. 7 shows the first wide-range STM image of Be(0001). So far, small areas (11 nm × 11 nm) have been imaged to analyze Friedel oscillations of a Be(0001) electronic surface state.[49] The wide-range STM images acquired during the present work reveal that the vast majority (90%) of apparent step heights is (3.2 ± 0.3) Å, which agrees reasonably well with the lattice parameter along the (0001) direction (3.6 Å). Step heights of 1.8 Å, i.e., half the lattice parameter along the surface normal, were less abundant. While a quantitative analysis of the distribution of step heights is beyond the scope of this work, we note that for the (0001) surface of alumina it has been shown that the statistical distribution of step heights depends on the details of sample preparation.[50]

B. Acoustic surface plasmon

The acoustic surface plasmon dispersion has been calculated for the $\bar{\Gamma}\bar{M}$ and $\bar{\Gamma}\bar{K}$ directions of the Be(0001) surface Brillouin zone.[15] However, it has been experimentally reported for the $\bar{\Gamma}\bar{M}$ direction only.[16] It was argued that along $\bar{\Gamma}\bar{K}$ interband transitions involving a Be(0001) surface state at $\bar{M}$
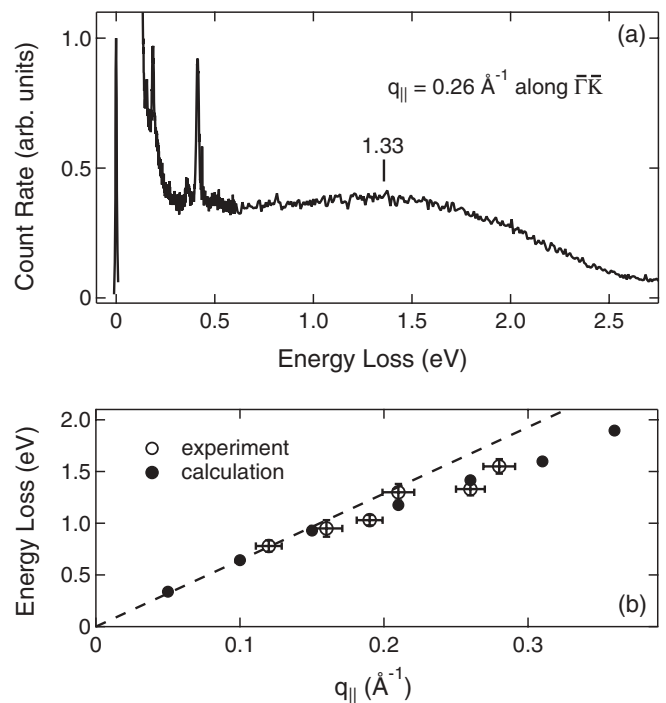
FIG. 8. (a) Electron energy loss spectrum acquired in off-specular scattering conditions with a momentum transfer of $q_{\parallel} = 0.26\,\text{Å}^{-1}$ along the $\bar{\Gamma}\bar{K}$ direction of the Be(0001) surface Brillouin zone (impact energy: 8 eV, count rate and FWHM of elastic peak: 90 × 10^3 s^{-1}, 7 meV). The loss spectrum was multiplied by 1700. The broad feature centered at 1.33 eV is due to the acoustic surface plasmon. Additional peaks between 0.15 and 0.45 eV originate from H and OH vibrations (see text). (b) Energy of the acoustic surface plasmon as a function of parallel momentum transfer along $\bar{\Gamma}\bar{K}$. Experimental data appear as circles. Calculated data have been adapted from Ref. 51 and are depicted as dots. The dashed line indicates an extrapolation of the linear dispersion from low to high parallel wave vectors. The slope is $\approx$6.4 eV Å^{-1} (Ref. 15).

have a more detrimental effect on the acoustic surface plasmon than along $\bar{\Gamma}\bar{M}$.[51] Spectroscopic signatures of the acoustic surface plasmon along $\bar{\Gamma}\bar{K}$ turned out to be rather weak and broad, which may be partly caused by the aforementioned reason and partly by the presence of adsorbates. A typical spectrum is shown in Fig. 8(a) for a momentum transfer of $q_{\parallel} = 0.26$ Å^{-1} along $\bar{\Gamma}\bar{K}$. The broad feature centered at 1.33 eV is interpreted as the signature of the acoustic surface plasmon. This assignment is corroborated by the agreement between experimental and calculated[51] dispersion data depicted in Fig. 8(b). To acquire angle-resolved vibration spectra the impact energy of electrons has been fixed to 8 eV and the analyzer has been rotated out of the specular scattering direction ($\vartheta = 65°$) by an angle φ ranging from $0°$ to $12°$. The parallel momentum transfer of an electron scattered from a vibrational excitation with energy $\hbar\omega$ and detected at an angle $\vartheta - \varphi$ with respect to the surface normal is calculated as

$$q_{\parallel} = \frac{\sqrt{2mE_0}}{\hbar}\left[\sin\vartheta - \sqrt{1 - \frac{\hbar\omega}{E_0}}\sin(\vartheta - \varphi)\right],$$

where E_0 denotes the energy of the incident electrons, m is the free electron mass, and $\hbar$ is the Planck constant divided by 2π. Based on the agreement between experimental and calculated data [Fig. 8(b)] the influence of the initial oxidation of Be(0001) on the dispersion of the acoustic surface plasmon is negligible. The slopes of the experimental and calculated dispersion curves for small parallel wave vectors are virtually identical. The dashed line in Fig. 8(b) depicts an extrapolation of the linear dispersion expected for small wave vectors to higher values of $q_{\parallel}$. The slope of this dispersion curve is given by the Fermi velocity of the Be(0001) surface state.[15] Possible explanations for the observed persistence of the acoustic surface plasmon are the following. Our calculations of the Be(0001) electronic structure indicate that the surface state of pristine Be(0001) at $\bar{\Gamma}$ shifts to lower energies upon increasing O coverage. At full coverage this surface state is completely filled, mainly by electron donation from O_B atoms. The data presented here were acquired from a Be(0001) surface which had been partly covered with oxygen. Therefore, the surface state at $\bar{\Gamma}$ is not completely occupied and still sustains the surface plasmon. Moreover, according to the calculations the surface state at $\bar{M}$ is not affected by the presence of oxygen and thus may support the occurrence of the acoustic surface plasmon. In contrast to the present findings, K adsorption on Be(0001) does lead to a modification of the slope of the dispersion curve, which has been attributed to K-induced quantum well states.[29]

Due to the low intensity of the plasmon losses long data acquisition times were necessary for an acceptable signal-to-noise ratio. The inevitable contamination of the Be(0001) surface leads to further loss features at 156, 185, 360, and 413 meV [Fig. 8(a)]. These signatures appeared with significant intensity in off-specular loss spectra, while in specular spectra they were hardly discriminated from the background. The comparison with previously reported results reveals that peaks at 156 and 185 meV may be assigned to vibration modes of atomic hydrogen.[39] The loss energies of 360 and 413 meV may be related to vibration modes of hydroxyl groups.[45,52] The presence of atomic hydrogen and hydroxyl groups on the initially oxidized Be(0001) surface is likely due to the dissociation of residual H_2O.[6,53] In Ref. 6 it has been shown that H dissociated from H_2O is trapped in the oxide layer.

IV. SUMMARY AND CONCLUSIONS

Inelastic electron scattering and density functional calculations unravel the geometric structure of Be(0001) in its initially oxidized state. The formed Be-O mixing layer reflects the strong reorganization of the light and reactive beryllium atoms when oxygen is adsorbed. The proposed atomic structure is supported by a fair agreement between experimental and calculated spectroscopic signatures of four distinct Be-O vibrational modes with respect to their energies and relative intensities. While the two topmost Be layers are considerably modified due to the presence of O atoms, the dispersion of the acoustic surface plasmon is not significantly affected.

ACKNOWLEDGMENT

*Present address: Institute of Physical Chemistry and Abbe Center of Photonics, Friedrich-Schiller-University Jena, D-07743 Jena, Germany; martin.jahn@uni-jena.de

†joerg.kroeger@tu-ilmenau.de

[1] H. H. Kung, *Transition Metal Oxides, Surface Chemistry and Catalysis* (Elsevier, Amsterdam, 1989).

[2] V. E. Heinrich and P. A. Cox, *The Surface Science of Metal Oxides* (Cambridge University Press, Cambridge, England, 1994).

[3] K. R. Lawless, Rep. Prog. Phys. **37**, 231 (1974).

[4] D. E. Fowler and J. M. Blakely, J. Vac. Sci. Technol. **20**, 930 (1982).

[5] D. E. Fowler and J. M. Blakely, Surf. Sci. **148**, 265 (1984).

[6] S. Zalkind, M. Polak, and N. Shamir, Surf. Sci. **385**, 318 (1997).

[7] Ch. Linsmeier and J. Wanner, Surf. Sci. **454–456**, 305 (2000).

[8] S. Zalkind, M. Polak, and N. Shamir, Surf. Sci. **513**, 502 (2002).

[9] R. Puchta, Nat. Chem. **3**, 416 (2011).

[10] K. L. Wilson, J. Vac. Sci. Technol. A **8**, 1750 (1990).

[11] S. Zalkind, M. Polak, and N. Shamir, Surf. Sci. **529**, 189 (2003).

[12] S. Zalkind, M. Polak, and N. Shamir, Surf. Sci. **601**, 1326 (2007).

[13] P. Zhang, B. Sun, and Y. Yang, Phys. Rev. B **79**, 165416 (2009).

[14] A. Allouche, J. Phys. Chem. C **115**, 8233 (2011).

[15] V. M. Silkin, A. Garcia-Lekue, J. M. Pitarke, E. V. Chulkov, E. Zaremba, and P. M. Echenique, Europhys. Lett. **66**, 260 (2004).

[16] B. Diaconescu, K. Pohl, L. Vattuone, L. Savio, P. Hofmann, V. M. Silkin, J. M. Pitarke, E. V. Chulkov, P. M. Echenique, D. Farías, and M. Rocca, Nature (London) **448**, 57 (2007).

[17] J. Ruvalds, Nature (London) **328**, 299 (1987).

[18] N. H. March and M. P. Tosi, Adv. Phys. **44**, 299 (1995).

[19]T. W. Ebbesen, H. J. Lezec, H. F. Ghaemi, T. Thio, and P. A. Wolff, Nature (London) **391**, 667 (1998).

[20]E. Ozbay, Science **311**, 189 (2006).

[21]V. M. Silkin, J. M. Pitarke, E. V. Chulkov, and P. M. Echenique, Phys. Rev. B **72**, 115435 (2005).

[22]V. M. Silkin, T. Nagao, V. Despoja, J. P. Echeverry, S. V. Eremeev, E. V. Chulkov, and P. M. Echenique, Phys. Rev. B **84**, 165416 (2011).

[23]S. J. Park and R. E. Palmer, Phys. Rev. Lett. **105**, 016801 (2010).

[24]K. Pohl, B. Diaconescu, G. Vercelli, L. Vattuone, V. M. Silkin, E. V. Chulkov, P. M. Echenique, and M. Rocca, Europhys. Lett. **90**, 57006 (2010).

[25]A. Traverse, T. Giradeau, C. Prieto, D. de Souse Meneses, and D. Zanghi, Europhys. Lett. **81**, 47001 (2008).

[26]A. Politano, A. R. Marino, V. Formoso, D. Farías, R. Miranda, and G. Chiarello, Phys. Rev. B **84**, 033401 (2011).

[27]S. Hüfner, *Photoelectron Spectroscopy* (Springer, Berlin, 1995).

[28]J. Algdal, T. Balasubramanian, M. Breitholtz, V. Chis, B. Hellsing, S.-Å. Lindgren, and L. Walldén, Phys. Rev. B **78**, 085102 (2008).

[29]V. M. Silkin, B. Hellsing, L. Walldén, P. M. Echenique, and E. V. Chulkov, Phys. Rev. B **81**, 113406 (2010).

[30]V. M. Silkin, E. V. Chulkov, J. P. Echeverry, and P. M. Echenique, Phys. Status Solidi B **247**, 1849 (2010).

[31]H. Ibach, J. Electron Spectrosc. Relat. Phenom. **64/65**, 819 (1993).

[32]J. P. Perdew, K. Burke, and M. Ernzerhof, Phys. Rev. Lett. **77**, 3865 (1996).

[33]J. P. Perdew, K. Burke, and M. Ernzerhof, Phys. Rev. Lett. **78**, 1396 (1997).

[34]P. Giannozzi, S. Baroni, N. Bonini, M. Calandra, R. Car, C. Cavazzoni, D. Ceresoli, G. L. Chiarotti, M. Cococcioni, I. Dabo, A. Dal Corso, S. de Gironcoli, S. Fabris, G. Fratesi, R. Gebauer, U. Gerstmann, C. Gougoussis, A. Kokalj, M. Lazzeri, L. Martin-Samos, N. Marzari, F. Mauri, R. Mazzarello, S. Paolini, A. Pasquarello, L. Paulatto, C. Sbraccia, S. Scandolo, G. Sclauzero, A. P. Seitsonen, A. Smogunov, P. Umari, and R. M. Wentzcovitch, J. Phys.: Condens. Matter **21**, 395502 (2009).

[35]N. Marzari, D. Vanderbilt, A. DeVita, and M. C. Payne, Phys. Rev. Lett. **82**, 3296 (1999).

[36]P. Rudolf, C. Astaldi, G. Cautero, and S. Modesti, Surf. Sci. **251-252**, 127 (1991).

[37]S.-A. Lindgren, C. Svensson, L. Walldén, A. Carlsson, and E. Wahlström, Phys. Rev. B **54**, 10912 (1996).

[38]J. Kröger, D. Bruchmann, S. Lehwald, and H. Ibach, Surf. Sci. **449**, 227 (2000).

[39]K. Ray, J. B. Hannon, and E. Plummer, Chem. Phys. Lett. **171**, 469 (1990).

[40]The partial pressure of H_2O in the vacuum recipient was 5×10^{-9} Pa according to mass spectra acquired prior to and after vibrational spectroscopy, while the O_2 signal fell below the detection limit of the mass spectrometer.

[41]K. Pohl, E. W. Plummer, S. V. Hoffmann, and P. Hofmann, Phys. Rev. B **70**, 235424 (2004).

[42]J. B. Hannon, E. J. Mele, and E. W. Plummer, Phys. Rev. B **53**, 2090 (1996).

[43]J. Kröger, S. Lehwald, and H. Ibach, Phys. Rev. B **58**, 1578 (1998).

[44]Constant-current STM images of clean Be(0001) that stayed under ultrahigh vacuum conditions for 60 h look similar.

[45]S. Völkening, K. Bedürftig, K. Jacobi, J. Wintterlin, and G. Ertl, Phys. Rev. Lett. **83**, 2672 (1999).

[46]V. Maurice, S. Cadot, and P. Marcus, Surf. Sci. **458**, 195 (2000).

[47]A. U. Goonewardne, J. Karunamuni, R. L. Kurtz, and R. L. Stockbauer, Surf. Sci. **501**, 102 (2002).

[48]W. X. Li, L. Österlund, E. K. Vestergaard, R. T. Vang, J. Matthiesen, T. M. Pedersen, E. Lægsgaard, B. Hammer, and F. Besenbacher, Phys. Rev. Lett. **93**, 146104 (2004).

[49]P. Sprunger, L. Petersen, E. W. Plummer, E. Lægsgaard, and F. Besenbacher, Science **275**, 1764 (1997).

[50]L. P. Van, O. Kurnosikov, and J. Cousty, Surf. Sci. **411**, 263 (1998).

[51]V. M. Silkin, J. M. Pitarke, E. V. Chulkov, B. Diaconescu, K. Pohl, L. Vattuone, L. Savio, Ph. Hofmann, D. Farías, M. Rocca, and P. M. Echenique, Phys. Status Solidi A **205**, 1307 (2008).

[52]A. M. Baró, J. Vac. Sci. Technol. **20**, 580 (1982).

[53]M. A. Gomez, L. R. Pratt, J. D. Kress, and D. Asthagiri, Surf. Sci. **601**, 1608 (2007).